Geophys. J. Int. (2005) **162,** 221–238 doi: 10.1111/j.1365-246X.2005.02608.x

The angular velocity of Nubia relative to Somalia and the location of the Nubia–Somalia–Antarctica triple junction

Benjamin C. Horner-Johnson,[1]* Richard G. Gordon,[1]† Sara M. Cowles[1]‡ and Donald F. Argus[2]

[1]*Department of Earth Science, Rice University, Houston, TX* 77005, *USA*
[2]*Jet Propulsion Laboratory, California Institute of Technology, Pasadena, CA* 91109, *USA*

Accepted 2005 February 7. Received 2004 December 2; in original form 2003 September 8

SUMMARY

A new analysis of geologically current plate motion across the Southwest Indian ridge (SWIR) and of the current location of the Nubia–Antarctica–Somalia triple junction is presented. Spreading rates averaged over the past 3.2 Myr are estimated from 103 well-distributed, nearly ridge-perpendicular profiles that cross the SWIR. All available bathymetric data are evaluated to estimate the azimuths and uncertainties of transform faults; six are estimated from multibeam data and 12 from precision depth recorder (PDR) data. If both the Nubian and Somalian component plates are internally rigid near the SWIR and if the Nubia–Somalia boundary is narrow where it intersects the SWIR, that intersection lies between ≈26°E and ≈32°E. Thus, the boundary is either along the spreading ridge segment just west of the Andrew Bain transform fault complex (ABTFC) or along some of the transform fault complex itself. These limits are narrower than and contained within limits of ≈24°E to ≈33°E previously found by Lemaux *et al.* from an analysis of the locations of magnetic anomaly 5. The data are consistent with a narrow boundary, but also consistent with a diffuse boundary as wide as ≈700 km. The new Nubia–Somalia pole of rotation lies ≈10° north of the Bouvet triple junction, which places it far to the southwest of southern Africa. The new angular velocity determined only from data along the SWIR indicates displacement rates of Somalia relative to Nubia of 3.6 ± 0.5 mm yr^{-1} (95 per cent confidence limits) towards 176° (S04° E) between Somalia and Nubia near the SWIR, and of 8.3 ± 1.9 mm yr^{-1} (95 per cent confidence limits) towards 121° (S59° E) near Afar. The new Nubia–Somalia angular velocity differs significantly from the Nubia–Somalia angular velocity estimated from Gulf of Aden and Red sea data. This significant difference has three main alternative explanations: (i) that the plate motion data have substantial unmodelled systematic errors, (ii) that the Nubian component plate is not a single rigid plate, or (iii) that the Somalian component plate is not a single rigid plate. We tentatively prefer the third explanation given the geographical distribution of earthquakes within the African composite plate relative to the inferred location of the Nubia–Somalia boundary along the SWIR.

Key words: Africa, diffuse plate boundary, Nubia, Somalia, Southwest Indian ridge, triple junction.

1 INTRODUCTION

The African composite plate comprises the Nubian component plate, the Somalian component plate and their mutual boundary (Royer & Gordon 1997; Gordon 1998; Fig. 1). In the African continent and Mozambique channel, the Nubia–Somalia boundary is the East African rift, along which occurs normal and strike-slip faulting, recent volcanism and topographic relief with extensional structures produced by horizontal stretching of the lithosphere (Baker 1972; Fairhead & Stuart 1982; Shudofsky 1985; Mohr 1987; Morley *et al.* 1992). The Southwest Indian ridge (SWIR), which spans 7700 km from the Bouvet triple junction (55°S, 0°E) northeastwards to the Rodrigues triple junction (25°S, 70°E) (Sclater *et al.* 1997), is a spreading centre that has traditionally been interpreted as the boundary between the African and Antarctic plates. Spreading across the SWIR is slow, with rates ranging from approximately 12 to 18 mm yr^{-1} (Chu & Gordon 1999). The transform faults that offset the SWIR are nearly everywhere left stepping and strike northeast (in the southwest) to due north (in the northeast; Fig. 2). The largest offset of the SWIR, ≈700 km, occurs along the Andrew Bain

*Now at: Portland State University, Portland, OR, USA
†Corresponding author. E-mail: rgg@rice.edu
‡Now at: Devon Energy, Houston, TX, USA

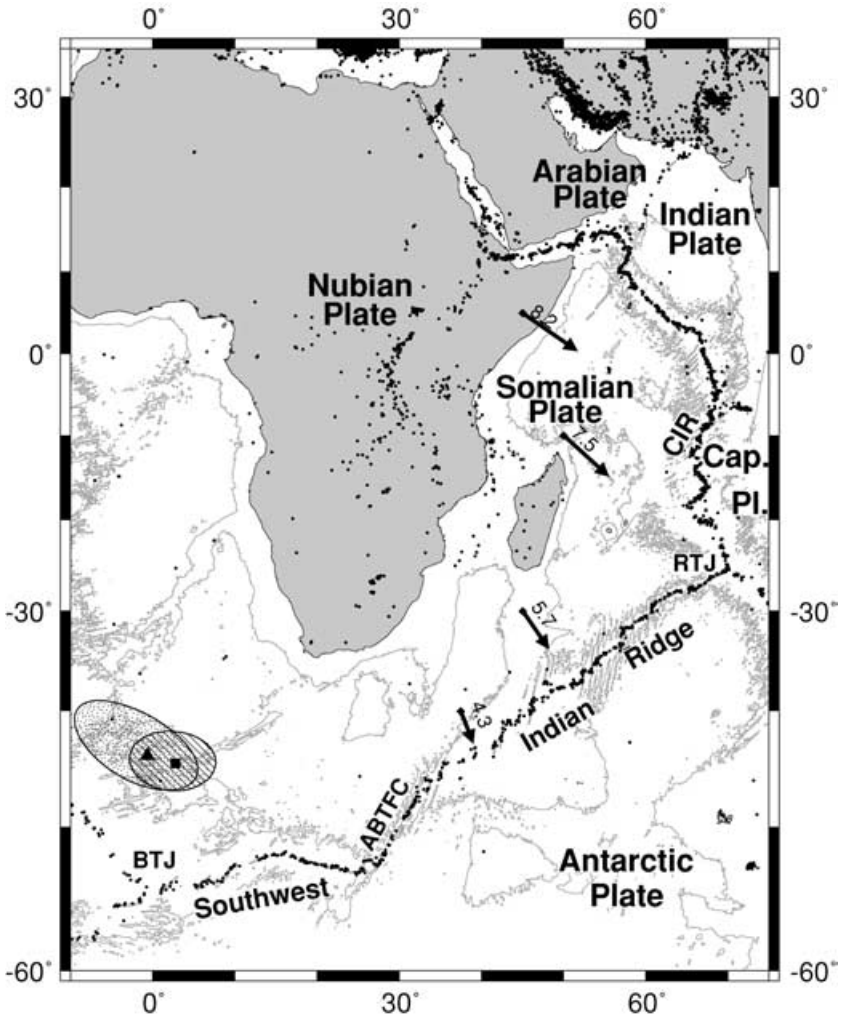

Figure 1. African continent, surrounding region, and our new Nubia–Somalia poles of rotation and 95 per cent confidence regions. Triangle and stippled ellipsoid: pole and 95 per cent confidence region estimated by differencing Nubia–Antarctica and Somalia–Antarctica best-fitting angular velocities assuming a narrow boundary intersecting the Southwest Indian ridge (SWIR) near 28°E. Square and diagonally striped ellipsoid: pole and 95 per cent confidence region estimated assuming the same narrow boundary along the SWIR but also incorporating data from the Gulf of Aden and from the Red sea (Chu & Gordon 1999). Black arrows: velocities of the Somalian Plate relative to an arbitrarily fixed Nubian Plate with rates in mm yr^{-1}. Bathymetry (light grey lines, 4000-m-depth contour) is from Smith & Sandwell (1997). Tiny black-filled circles show earthquake epicentres (1964–1998; Engdahl *et al.* 1998). Abbreviations: ABTFC, Andrew Bain transform fault complex; BTJ, Bouvet triple junction; RTJ, Rodrigues triple junction; CIR, Central Indian ridge; Cap. Pl., Capricorn Plate.

transform fault complex (ABTFC), which is a series of three active transform faults separated by small extensional offsets (Fisher & Goodwillie 1997; Sclater *et al.* 1997). The ABTFC separates the SWIR into two portions; the portion east of the ABTFC is approximately twice as long as the portion west of the ABTFC.

It has long been speculated that the Nubia–Somalia plate boundary continues south of Africa and intersects the SWIR (Chase 1978; Stein & Gordon 1984; DeMets *et al.* 1988, 1990; Jestin *et al.* 1994). From an analysis of plate motion data, Chu & Gordon (1999) showed that the Nubia–Somalia plate boundary did indeed intersect the SWIR, but from their 59 spreading rates and nine transform fault azimuths, they were unable to precisely locate that intersection. They speculated that the Nubia–Somalia plate boundary may be very wide where it intersects the SWIR, as suggested mainly by two observations. First, the best-fitting hypothetical narrow boundary (which in their analysis intersects the SWIR between 35.05°E and 38.50°E) has no obvious expression in the topography or seismicity of the African seafloor flanking the SWIR. Secondly, the only recorded earthquake between Africa and the SWIR with a magnitude greater than 5.5 was a thrust event ($M_w = 6.8$) that occurred far outside the confidence limits of the hypothesized narrow boundary.

Lemaux *et al.* (2002) used 237 locations of magnetic anomaly 5 (11 Ma) to estimate the displacement since 11 Ma between the Antarctic, Nubian and Somalian plates and to place bounds on the location of their triple junction. They found that the displacement between Nubia and Somalia near the SWIR since 11 Ma (23 ± 6 km; all numbers following ± signs herein are 95 per cent confidence limits) has been several times greater than that since 3.2 Ma (7 ± 2 km; Lemaux *et al.* 2002). Moreover, most of the motion between Nubia and Somalia near the SWIR since 11 Ma could have been accommodated in a relatively narrow zone that lies approximately 500 km west of the hypothetical narrow boundary indicated by the results of Chu & Gordon (1999). Their result led Lemaux *et al.* (2002) to propose that the main locus of the Nubia–Somalia boundary is along the putatively inactive African continuation of the ABTFC, which intersects the SWIR near 32°E. The estimated pole of rotation of Lemaux *et al.* (2002) for Nubia relative to Somalia lies significantly west of Chu & Gordon's (1999) pole of rotation.

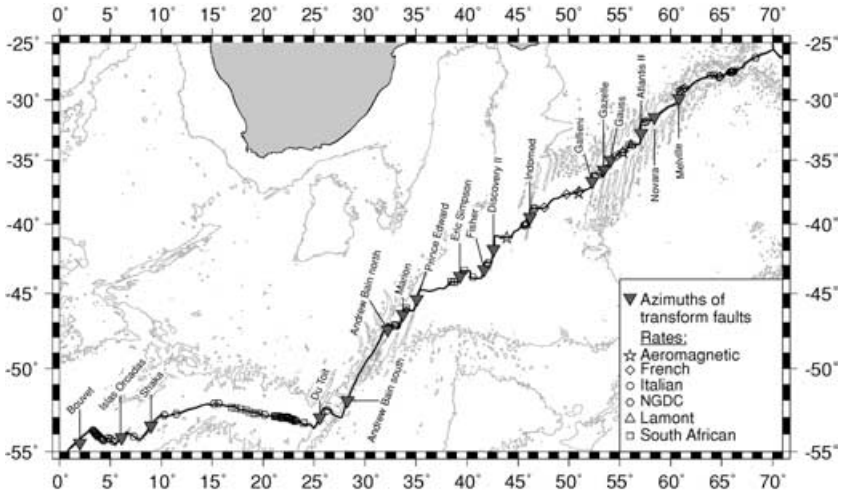

Figure 2. Map showing the locations along the Southwest Indian ridge (SWIR) of the spreading rates (open symbols) and transform fault azimuths (shaded inverted triangles) from ship and aeromagnetic surveys used in this study. The grey lines are the 4000-m-depth contour from Smith & Sandwell (1997).

The differences between the results of Chu & Gordon (1999) and those of Lemaux *et al.* (2002) raise several questions including the following. Is the Nubia–Somalia boundary currently narrow or diffuse near the SWIR? Does it intersect the SWIR along the Andrew Bain fracture zone complex as indicated by the results of Lemaux *et al.* (2002), or east of the Prince Edward fracture zone as indicated by the results of Chu & Gordon (1999)? Does the pole of current rotation lie near the east coast of South Africa or much farther west? Here, to address these questions, we present an analysis of a new set of spreading rates (averaged over the past 3.2 Myr) and transform fault azimuths that are greater in number and typically of higher quality than those used by Chu & Gordon (1999).

2 METHODS

2.1 Rates of seafloor spreading

Each relevant profile segment is projected perpendicular to the segment of the SWIR that it crosses. An exception is a group of 13 profiles near the Bouvet triple junction that cross the ridge at a high angle (Ligi *et al.* 1999). To project these 13 profiles perpendicular to the ridge would not be useful, but the profiles are spaced close enough to one another that we were able to construct a 1-arcmin grid of the crustal magnetization. We resampled this grid along 12 great circle segments perpendicular to the strike of the ridge and used these constructed profiles to estimate spreading rates.

The azimuth of each SWIR segment (or subsegment for long segments) is estimated from the mean azimuth of the anomaly 2A isochrons on both sides of the ridge. The projected profile segments were then compared with synthetic magnetic anomaly profiles with rates ranging from 8 to 18 mm yr^{-1} (Figs 3, 4, 5, 6 and 7). The synthetic magnetic anomaly profiles were calculated assuming a magnetic reversal transition width of 2 km, skewness values appropriate for ridge azimuth and latitude of the relevant segment of the SWIR, the geomagnetic reversal timescale of Cande & Kent (1995), and a depth to source of 3.5 km for shipboard profiles and a depth to source of 10.5 km for airplane profiles. The spreading rate that we estimate for each profile generally is the rate used to

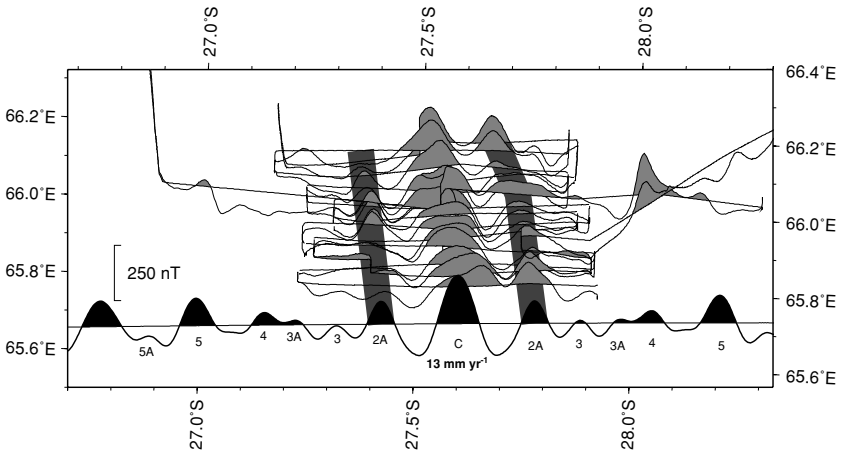

Figure 3. Magnetic profiles (reduced to the pole) crossing the Southwest Indian ridge (SWIR) between 65.5°E and 66.5°E. Grey shading indicates normal polarity on the observed profiles. Black shading indicates normal polarity on a synthetic magnetic anomaly profile calculated for a full spreading rate of 13 mm yr^{-1}. Numerals beneath the synthetic profile are magnetic anomaly numbers. The dark grey bars show magnetic anomaly 2A. Oblique Mercator projection about the best-fitting Somalia–Antarctica pole of rotation (Table 4). If seafloor spreading has been orthogonal, the magnetic anomalies would align vertically on this projection. Instead they make an angle of ≈10° with the vertical, indicating that spreading has been ≈10° oblique.

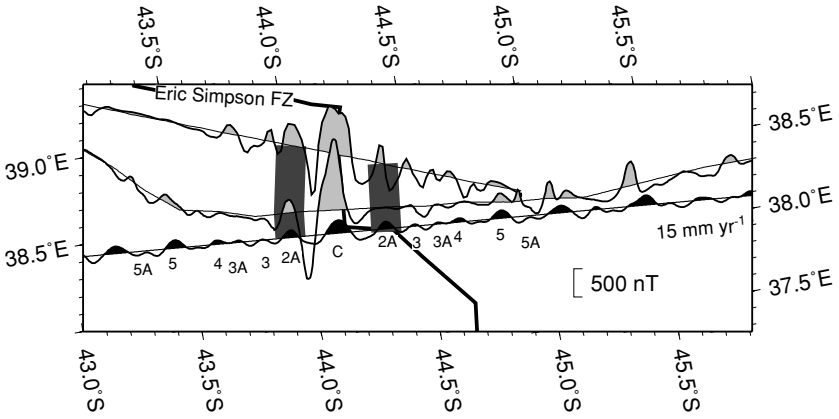

Figure 4. Magnetic profiles (reduced to the pole) crossing the Southwest Indian ridge (SWIR) between 37.5°E and 39.5°E. Grey shading indicates normal polarity on the observed profiles. Black shading indicates normal polarity on a synthetic magnetic anomaly profile calculated for a full spreading rate of 15 mm yr^{-1}. Numerals beneath the synthetic profiles are magnetic anomaly numbers. The dark grey bars show magnetic anomaly 2A. The location of the ridge and transform system is shown by the heavy line. Oblique Mercator projection about the best-fitting Somalia–Antarctica pole of rotation (Table 4).

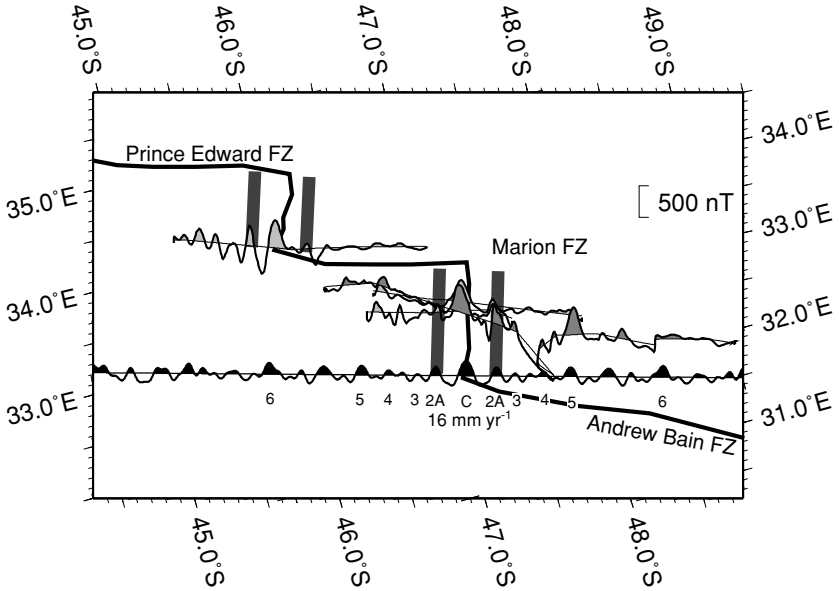

Figure 5. Magnetic profiles (reduced to the pole) crossing the Southwest Indian ridge (SWIR) between 32°E and 35°E. Grey shading indicates normal polarity on the observed profiles. Black shading indicates normal polarity on a synthetic magnetic anomaly profile calculated for a full spreading rate of 16 mm yr^{-1}. Numerals beneath the synthetic profiles are magnetic anomaly numbers. The dark grey bars show magnetic anomaly 2A. The location of the ridge and transform system is shown by the heavy line. Oblique Mercator projection about the best-fitting Somalia–Antarctica pole of rotation (Table 4).

construct the synthetic magnetic anomaly profile that best fit the distance between magnetic anomaly 2A on both sides of the SWIR. For longer profiles, the fit to the distance to anomalies over older seafloor, especially anomaly 5, is also considered.

The 1σ uncertainty assigned to all the spreading rates is estimated from the dispersion of the rates from the relevant rates-only data set. This procedure is consistent with the methods used to estimate uncertainties for finite rotations of plates (Chang 1988), but runs the risk of underestimating the uncertainties in rotational parameters unless errors in estimated rates from profiles near one another are uncorrelated, which is probably not true.

2.2 Azimuths of transform faults

Transform fault azimuths are estimated from bathymetric data. The width of the transform is the narrowest morphotectonic element that could be inferred from the available data. Errors assigned to transform faults are based on the geometry of the imaged morphotectonic feature:

$$\sigma = \frac{\tan^{-1}(W/L)}{\sqrt{3}}, \tag{1}$$

where W is the width of the narrowest tectonic element insonified and L is the insonified length of the transform fault (DeMets *et al.* 1994).

2.3 Location of the Nubia–Somalia–Antarctica triple junction

We use spreading rates and transform fault azimuths to estimate the relative motion across the SWIR using methods that we have used many times before (e.g. DeMets *et al.* 1990). We first analyse each

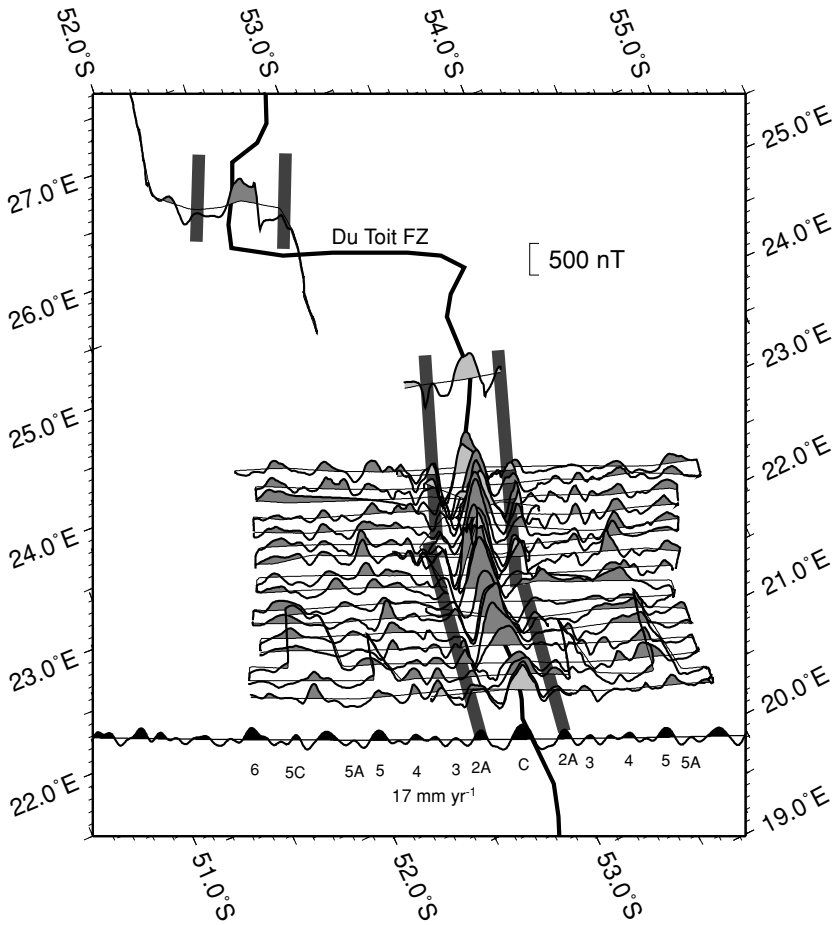

Figure 6. Magnetic profiles (reduced to the pole) crossing the Southwest Indian ridge (SWIR) between 21°E and 27°E. Shading indicates normal polarity on the observed profiles. Black shading indicates normal polarity on a synthetic magnetic anomaly profile calculated for a full spreading rate of 17 mm yr^{-1}. Numerals beneath the synthetic profiles are magnetic anomaly numbers. The dark grey bars show magnetic anomaly 2A. The location of the ridge and transform system is shown by the heavy line. Oblique Mercator projection about the best-fitting Nubia–Antarctica pole of rotation (Table 4). If seafloor spreading has been orthogonal, the magnetic anomalies would align vertically on this projection. Instead they make an angle of ≈10° with the vertical, indicating that spreading has been ≈10° oblique.

data type separately and then repeat the analysis on the combined data.

Initially, the data are hypothetically assumed to record the motion of Africa relative to Antarctica and the best-fitting angular velocity and associated value of chi-square are estimated for this two-plate model. Next a three-plate model is constructed with a narrow boundary between Nubia and Somalia assumed to lie between the two westernmost data along the SWIR; chi-square is determined for this three-plate model by finding the best-fitting angular velocities for both Nubia and Somalia relative to Antarctica; the values of chi-square for each of these two best-fitting angular velocities are summed to obtain chi-square for this assumed triple junction location. The assumed triple junction location is then shifted eastwards along the SWIR by reassigning the westernmost remaining Somalian–Antarctic datum as the easternmost Nubian–Antarctic datum; chi-square for this three-plate model is determined. We repeat this process until all data are reassigned as Nubian–Antarctic data and chi-square has consequently been determined for $N - 1$ three-plate models, where N is the number of data.

The hypothetical location of the Nubia–Antarctica–Somalia triple junction that results in the lowest value of chi-square is taken to be the best estimate of the triple junction location. An F-ratio test is used to determine if the best-fitting three-plate model (with separate Nubian and Somalian plates spreading away from Antarctica) significantly improves the fit to the data compared with the two-plate model of a single African Plate spreading away from Antarctica:

$$F_{\text{best}} = \frac{\left(\chi_2^2 - \chi_{3,\text{min}}^2\right)/(m+1)}{\chi_{3,\text{min}}^2/[N-(2m+1)]}, \tag{2}$$

where χ_2^2 is chi-square for the Africa–Antarctica two-plate model, $\chi_{3,\text{min}}^2$ is chi-square for the three-plate model with the triple junction location resulting in the lowest value of chi-square and N is the number of data. m equals 2 if only transform fault azimuths are used and equals 3 if only spreading rates or both spreading rates and transform fault azimuths are used (Stein & Gordon 1984). The addition of 1 to m or to $2m$ is as a result of the other adjustable parameter, which is the assumed longitude of the Nubia–Antarctica–Somalia triple junction.

3 PLATE MOTION DATA

3.1 Rates of seafloor spreading

We initially examined many magnetic profiles from the National Geophysical Data Center and other sources. With the exception of the gridded and resampled profiles near the Bouvet triple junction

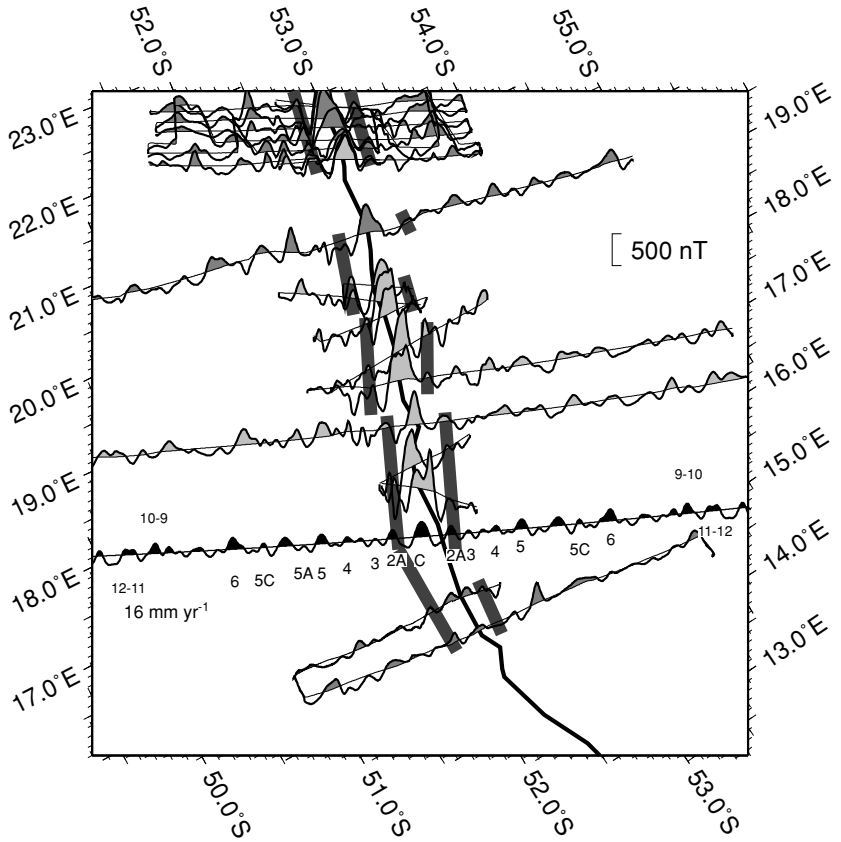

Figure 7. Magnetic profiles (reduced to the pole) crossing the Southwest Indian ridge (SWIR) between 14°E and 23°E. Shading indicates normal polarity on observed profiles. Black shading indicates normal polarity on a synthetic magnetic anomaly profile calculated for a full spreading rate of 16 mm yr^{-1}. Numerals beneath the synthetic profiles are magnetic anomaly numbers. The dark grey bars show magnetic anomaly 2A. The location of the ridge and transform system is shown by the heavy line. Oblique Mercator projection about the best-fitting Nubia–Antarctica pole of rotation (Table 4). If seafloor spreading has been orthogonal, the magnetic anomalies would align vertically on this projection. Instead they make an angle of ≈10° with the vertical, indicating that spreading has been ≈10° oblique.

mentioned above, profile segments crossing the ridge were given further consideration only if they crossed magnetic anomaly 2A on both sides of the ridge before crossing any fracture zones or non-transform offsets and made an angle with the ridge perpendicular of less than 25°. We also rejected profiles located where we interpreted propagating rifts that affected the location of anomaly 2A; in particular, we rejected a group of closely spaced profiles east of the Prince Edward fracture zone (between 35.9°E and 36.6°E) that would otherwise meet our criteria. We furthermore rejected 12 profiles between 11.70°E and 14.97°E along which highly oblique spreading apparently occurs, with the ridge-perpendicular direction being ≈33° to ≈45° counter-clockwise of the direction of plate motion. The rates that we estimated for these 12 profiles were systematically too high for our interpretation of the ridge strike to be correct. Perhaps spreading there is more nearly orthogonal than we estimated, with the apparent oblique spreading being a consequence of many small offsets of the spreading ridge (*cf.* Fisher & Goodwillie 1997). In the end, this left 91 high-quality, nearly ridge-perpendicular profiles plus 12 profiles constructed from the gridded data. The resulting spreading rate data set contains 103 well-distributed spreading rates (Table 1).

3.2 Azimuths of transform faults

Azimuths of transform faults were estimated from multibeam data for six transform faults and from precision depth recorder (PDR) data for 12 transform faults (Table 2; Dick *et al.* 1991; Mendel *et al.* 1997, Sclater *et al.* 1997; Sclater, personal communication, 2000). The narrowest tectonic element that could be imaged from PDR data is the entire transform valley, which ranges in width from 12 to 18 km (Table 2). Narrower features, which we assume contain the entire zone of active faulting and are 4 to 6 km wide, were resolvable from multibeam data along six transform fault segments. Four of these six were inferred from the presence of bright reflectors and the other two (Novara and Melville) were inferred from the presence of a narrower valley contained within the transform valley. The new set of 18 transform fault azimuths provides a much better distributed and more reliable set of azimuths than was available before (Table 2).

4 RESULTS

4.1 Triple junction location

4.1.1 Spreading rates

The best-fitting location for the intersection of a hypothetical narrow Nubia–Somalia boundary with the SWIR is anywhere between 26.31°E and 32.89°E (excluding the endpoints); this longitude range is bounded on the west by the one spreading rate observed between the Du Toit transform fault and the southern Andrew Bain transform fault and on the east by the westernmost spreading rates east of the northern Andrew Bain transform fault (Fig. 8). The standard deviation of the spreading rates is 0.6 mm yr^{-1}. An F-ratio test indicates

Table 1. Southwest Indian ridge (SWIR) anomaly 2A spreading rates.

Lat. (°N)	Lon. (°E)	Prof. azim.	Ridge ⊥ azim.	Rate (mm yr^{-1})	Profile ID	Data source
−53.77	3.27	N43E	N48E	15.9	synth_3.27	Italian
−53.82	3.36	N43E	N48E	15.7	synth_3.36	Italian
−53.87	3.44	N43E	N48E	14.9	synth_3.44	Italian
−53.95	3.47	N61E	N48E	15.3	ch115l03.07	NGDC
−53.92	3.53	N43E	N48E	14.9	synth_3.53	Italian
−53.97	3.62	N43E	N48E	14.0	synth_3.62	Italian
−54.02	3.71	N43E	N48E	14.9	synth_3.71	Italian
−54.14	3.72	N32E	N48E	14.7	rsa75-3	NGDC
−54.07	3.80	N43E	N42E	14.5	synth_3.80	Italian
−54.17	3.98	N43E	N42E	15.0	synth_3.98	Italian
−54.22	4.07	N43E	N42E	16.0	synth_4.07	Italian
−54.27	4.16	N43E	N40E	15.0	synth_4.16	Italian
−54.32	4.25	N43E	N42E	15.0	synth_4.25	Italian
−54.35	4.32	N43E	N42E	15.0	synth_4.32	Italian
−54.22	4.80	N40E	N40E	15.0	a2107l06.04	NGDC
−54.28	5.03	N42E	N40E	15.0	i1176.04	NGDC
−54.41	5.29	N41E	N40E	16.0	i1176.03	NGDC
−54.14	7.30	N37E	N42E	16.0	i1176.05	NGDC
−52.89	10.28	N42E	N29E	15.7	v2905.2	NGDC
−52.81	11.47	N21E	N28E	17.0	i1176.15	NGDC
−52.18	15.17	N08E	N15E	16.9	rsa72-2.07	NGDC
−52.17	15.63	N05E	N15E	15.8	rsa72-2.08	NGDC
−52.42	16.94	N36E	N15E	16.0	hb310.1a	So.Afr.
−52.44	17.30	N00E	N15E	16.5	hb309.1a	So.Afr.
−52.51	17.77	N21E	N15E	16.0	hb221.1a	So.Afr.
−52.57	18.33	N17E	N15E	15.0	hb213.1a	So.Afr.
−52.70	18.64	N03W	N15E	16.7	hb316.1a	So.Afr.
−52.78	19.11	N00E	N13E	14.9	hb214.1a	So.Afr.
−52.77	19.28	N28E	N13E	16.0	hb319.1a	So.Afr.
−52.77	19.51	N31E	N10E	15.1	saa022.9	So.Afr.
−52.87	20.16	N11E	N10E	17.0	i1277	NGDC
−52.95	21.14	N16E	N10E	17.2	saa022.16	So.Afr.
−52.94	21.15	N23E	N10E	16.8	ag044l01.16	NGDC
−52.96	21.29	N23E	N10E	17.0	ag044l01.15	NGDC
−52.97	21.40	N23E	N10E	17.0	ag044l01.14	NGDC
−52.97	21.58	N23E	N10E	16.8	ag044l01.13	NGDC
−53.00	21.68	N23E	N10E	16.8	ag044l01.12	NGDC
−53.01	21.83	N23E	N10E	17.0	ag044l01.11	NGDC
−53.03	21.84	N26E	N10E	17.3	saa022.18	So.Afr.
−53.04	21.98	N23E	N10E	17.0	ag044l01.10	NGDC
−52.99	22.15	N23E	N20E	17.0	ag044l01.09	NGDC
−52.99	22.27	N23E	N20E	17.0	ag044l01.08	NGDC
−53.02	22.43	N23E	N20E	17.0	ag044l01.07	NGDC
−53.05	22.45	N18E	N20E	17.0	saa022.21	So.Afr.
−53.05	22.55	N22E	N20E	17.0	ag044l01.06	NGDC
−53.10	22.71	N23E	N20E	17.0	ag044l01.05	NGDC
−53.11	22.83	N22E	N20E	17.0	ag044l01.04	NGDC
−53.14	22.86	N20E	N20E	17.5	saa022.22	So.Afr.

that the model with separate Nubian and Somalian plates divided at the best-fitting location fits the spreading rates significantly better than does the model with a single African Plate. The statistic, F, equals 23.8. The probability, p, of F being this large or larger by chance is only 1×10^{-13}. The 95 per cent confidence limits of the best-fitting triple junction location are the same as the interval quoted above for the best-fitting location.

The best-fitting angular velocities indicate that Nubia–Antarctica spreading rates increase from approximately 15 mm yr^{-1} near the Bouvet triple junction to approximately 18 mm yr^{-1} near the ABTFC and that Somalia–Antarctica spreading rates increase from approximately 13 mm yr^{-1} near the Rodrigues triple junction to approximately 14 mm yr^{-1} near the ABTFC (Fig. 9).

If the Nubia–Somalia boundary is narrow and its location is not inferred from our plate motion data, but instead is specified by independent data, independent reasoning, or both, the fit to the data of the corresponding three-plate Nubia–Antarctica–Somalia model would be significantly better than the fit to a two-plate Africa–Antarctica model if chi-square for the three-plate model is below the thinner horizontal dashed line in Fig. 8. This criterion is satisfied by many hypothetical triple junction locations along the SWIR (from 4.32 °E to 65.83°E). In particular, if the Nubia–Somalia boundary follows the inactive African continuation of the ABTFC, as proposed by Lemaux *et al.* (2002), the data are fit significantly better ($F = 32.0$, $p = 1.8 \times 10^{-13}$) by a three-plate model ($\chi^2 = 95.846$, $\nu = 97$) than by a two-plate model. Alternatively, if the boundary

Table 1. *(Continued.)*

Lat. (°N)	Lon. (°E)	Prof. azim.	Ridge ⊥ azim.	Rate (mm yr^{-1})	Profile ID	Data source
−53.17	23.04	N22E	N20E	17.0	ag044l01.02	NGDC
−53.22	23.15	N24E	N20E	16.8	saa022.20	So.Afr.
−53.22	23.20	N23E	N20E	17.0	ag044l01.01	NGDC
−53.35	24.00	N12E	N20E	18.0	saa022.23	So.Afr.
−52.59	26.31	N23E	N22E	18.0	prot05mv.01	NGDC
−47.20	32.89	N29E	N16E	15.0	prot05mv.04	NGDC
−47.20	32.92	N16E	N16E	15.0	ag053.3	So.Afr.
−47.23	33.00	N15E	N16E	15.0	ag053.2	So.Afr.
−46.02	34.00	N14E	N15E	15.0	ag053.33	So.Afr.
−44.18	38.43	N04E	N05E	15.5	rsa72ma.3	So.Afr.
−44.20	38.77	N22E	N05E	15.0	saa76_11a.16	So.Afr.
−43.38	39.73	N25E	N03E	15.1	saa76_11a.1b	So.Afr.
−43.86	40.56	N12E	N06E	15.3	md34.17	NGDC
−42.88	42.02	N14W	N06E	14.3	prot05mv.11	NGDC
−41.04	43.90	N09E	N01W	14.9	0550-073.c2.Td	Pr.Mag.
−40.10	45.61	N01W	N01W	15.0	inmd08mv.04	NGDC
−40.09	45.77	N00E	N01W	14.0	vem1605.2	Lamont
−40.06	45.78	N05W	N01W	15.0	md05.3	French
−38.84	46.51	N07E	N02W	16.1	prot05mv.14	NGDC
−38.79	46.69	N04E	N02W	15.0	inmd08mv.03	NGDC
−38.75	47.59	N21W	N02W	14.1	ga02.7	French
−37.72	49.77	N11W	N05W	13.9	md01.2	French
−37.64	50.94	N10W	N07W	14.2	0480-301.c1.Td	Pr.Mag.
−37.48	51.02	N00E	N07W	13.9	md47.1	French
−36.07	53.09	N00E	N02E	13.5	ga00.3	French
−34.71	54.61	N03E	N01W	14.3	md34.09	NGDC
−34.37	55.30	N00E	N01W	13.0	md34.08	NGDC
−34.39	55.34	N00E	N01W	14.1	0480-301.c2.Td	Pr.Mag.
−33.76	55.91	N00E	N02W	13.0	md34.05	NGDC
−33.77	56.10	N09W	N02W	14.0	vem1605.4	Lamont
−33.78	56.26	N02E	N02W	13.0	md34.06	NGDC
−31.88	57.40	N02W	N05W	15.2	a2093l05.02	NGDC
−31.80	57.63	N00E	N04W	14.3	md34.02	NGDC
−29.23	60.89	N01W	N14W	14.1	v2903	NGDC
−29.07	61.17	N14W	N14W	13.5	antp07mv.10	NGDC
−28.98	61.39	N18W	N14W	14.0	ga00.4	French
−27.84	63.89	N03W	N09W	13.5	a2093l05.09	NGDC
−27.86	64.21	N03W	N09W	14.5	a2093l05.10	NGDC
−27.98	64.74	N00E	N06W	14.1	a2093l05.11	NGDC
−27.95	64.82	N00E	N06W	14.0	md37.1	French
−27.60	65.80	N02W	N09W	13.2	84001211.16	NGDC
−27.60	65.83	N01W	N09W	14.2	84001211.03	NGDC
−27.59	65.86	N03W	N09W	13.7	84001211.17	NGDC
−27.58	65.90	N00E	N10W	14.2	84001211.18	NGDC
−27.58	65.92	N04W	N10W	13.1	84001211.04	NGDC
−27.57	65.95	N02W	N10W	13.2	84001211.19	NGDC
−27.56	65.98	N04W	N10W	12.6	84001211.05	NGDC
−27.54	66.00	N02E	N10W	12.8	a2093l05.13	NGDC
−27.56	66.00	N03W	N10W	13.1	84001211.20	NGDC
−27.54	66.04	N01W	N10W	13.2	84001211.21	NGDC
−27.53	66.06	N03W	N10W	13.7	84001211.06	NGDC
−27.52	66.10	N03W	N10W	14.2	84001211.22	NGDC
−27.52	66.15	N02W	N10W	12.7	84001211.23	NGDC
−27.50	66.18	N05W	N10W	14.6	84001211.07	NGDC
−26.28	68.33	N03W	N08W	12.4	a2093l06.04	NGDC

intersects the SWIR between 37.20°E and 38.50°E (the best-fitting Nubia–Somalia narrow boundary location of Chu & Gordon 1999), the data are also fit significantly better ($F = 11.5$, $p = 1.6 \times 10^{-6}$) by a three-plate model ($\chi^2 = 140.646$, $\nu = 97$) than by a two-plate model (Table 3).

If the best-fitting Somalia–Antarctica angular velocity is used to predict spreading rates west of the ABTFC, the predicted rates are systematically lower than those observed. On the other hand, the Nubia–Antarctica angular velocity predicts rates east of the ABTFC that are systematically higher than those observed (Fig. 9).

4.1.2 Azimuths of transform faults

The 18 transform fault azimuths were analysed similarly to the spreading rates. The best-fitting location along the SWIR for a

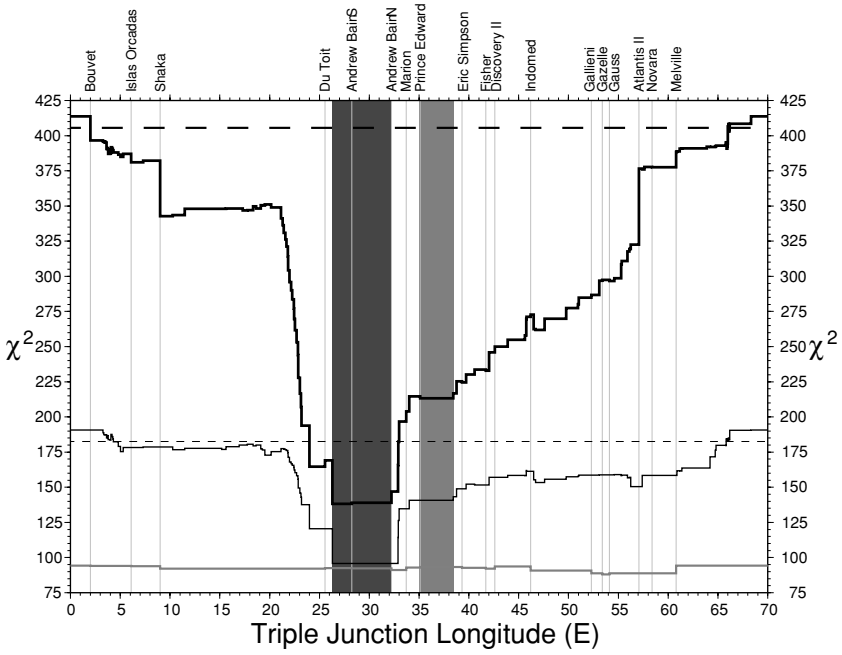

Figure 8. Sum-squared normalized misfit versus longitude of the intersection of the Southwest Indian ridge (SWIR) with a hypothetical narrow boundary between Nubia and Somalia. Thin black curve is the results from spreading rate data; grey curve (i.e. the lowest curve) is the results from transform fault azimuths, with χ^2 offset by 75 (i.e. the actual values range from 13.0 to 19.3); bold black curve is the results from combined spreading rate and transform fault azimuth data. The dashed horizontal lines show the significance thresholds for boundaries hypothesized from independent data or reasoning; the thin dashed line is for rates only and the thick dashed line is for rates plus transform fault azimuths. The lighter grey shaded region is the 95 per cent confidence limits of the narrow Nubia–Somalia boundary of Chu & Gordon (1999). The darker grey shaded region is the 95 per cent confidence limits for the narrow Nubia–Somalia boundary for the combined spreading rate and transform fault azimuth data. The light grey vertical lines show the longitudes of the transform fault azimuths in Table 2.

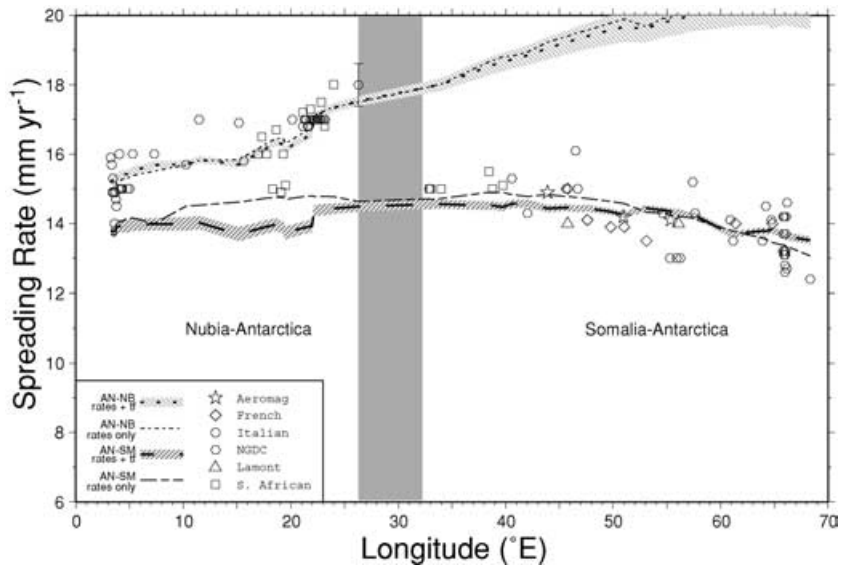

Figure 9. Comparison of observed seafloor spreading rates with those calculated assuming a narrow Nubia–Somalia boundary intersecting the Southwest Indian ridge (SWIR) near 28°E. Dark grey shading shows the 95 per cent confidence limits for the best-fitting narrow Nubia–Somalia boundary. Dotted curve: rates calculated from the angular velocity (0.183° ± 0.012° Myr^{-1} about 13.0°S, 29.8°W) that best fits spreading rates and transform fault azimuths west of 28°E, corresponding to Nubia–Antarctica motion; light grey diagonal stripes show 1σ uncertainty. Short dash-dot curve: rates calculated from the angular velocity that best fits the spreading rates west of 28°E. Dashed curve: rates calculated from the angular velocity (0.131° ± 0.002° Myr^{-1} about 6.8°N, 42.5°W) that best fits spreading rates and transform fault azimuths east of 28°E, corresponding to Somalia–Antarctica motion; dark grey diagonal stripes show 1σ uncertainty. Long dash-short dash curve: rates calculated from the angular velocity that best fits the spreading rates east of 28°E.

narrow Nubia–Somalia boundary is anywhere between the Gazelle (53.4°E) and Gauss (54.1°E) transform faults, which is ≈21° to ≈27° farther east than the best-fitting location inferred from the spreading rates. No matter where we assume the Nubia–Somalia boundary intersects the SWIR, the data are fit insignificantly better by a three-plate model than by a two-plate model ($F = 2.1$, with 3 versus 13 degrees of freedom, $p = 0.15$ for the best-fitting three-plate model compared with the two-plate model; Figs 8 and 10).

Table 2. Southwest Indian ridge (SWIR) transform faults.

Lat. (° N)	Lon. (° E)	Azim. (°)	σ (°)	W (km)	L (km)	Offset (km)	FZ name	Technique	Bathymetric data source
−54.5	2.0	44.0	1.128	15	170	190	Bouvet	PDR	1
−54.2	6.1	41.0	2.374	15	80	100	Islas Orcadas	PDR	1
−53.5	9.0	39.0	1.089	15	180	200	Shaka	PDR	1
−53.02	25.55	22.0	0.661	5	95	115	Du Toit	SeaBeam	2
−52.0	28.25	20.0	2.296	18	100	270	Andrew Bain S	PDR	2
−47.48	32.24	16.0	1.167	6	65	240	Andrew Bain N	SeaBeam	2
−46.45	33.72	17.0	0.739	5	85	140	Marion	SeaBeam	2
−45.4	35.1	14.0	1.089	12	140	160	Prince Edward	PDR	1
−43.8	39.3	13.0	2.840	18	80	100	Eric Simpson	PDR	1
−43.3	41.7	10.0	1.907	15	100	120	Fisher	PDR	1
−41.9	42.6	07.0	1.012	15	190	210	Discovery II	PDR	1
−39.5	46.2	05.0	1.907	15	100	120	Indomed	PDR	1
−36.7	52.3	03.0	1.634	12	95	115	Gallieni	PDR	1
−35.8	53.4	03.0	2.529	12	60	80	Gazelle	PDR	1
−35.0	54.1	06.0	4.630	15	40	60	Gauss	PDR	1
−32.78	57.07	00.5	0.272	4	179	199	Atlantis II	SeaBeam	3
−31.45	58.4	−01.0	3.502	5	18	35	Novara	Multibeam	4
−29.85	60.8	−04.0	1.284	5	50	70	Melville	Multibeam	4

Legend: lat., latitude; lon., longitude; azim., azimuth of transform fault; σ, uncertainty in azimuth (eq. 1); W, width of the narrowest tectonic feature insonified; L, insonified length of the transform fault; offset, total distance between the ridge segment ends; FZ, fracture zone; PDR, precision depth recorder. References: (1) Sclater *et al.* (1997); (2) Sclater, personal communication (2000); (3) Dick *et al.* (1991); (4) Mendel *et al.* (1997).

Table 3. χ^2 and ν for subsets of our data along the Southwest Indian ridge (SWIR).

Plate pair	Data type	χ^2	ν
Africa–Antarctica	Spreading rates	190.7	100
Africa–Antarctica	Transform fault azimuths	19.3	16
Africa–Antarctica	Spreading rates and transform fault azimuths	413.7	118
	Best-fitting Narrow Boundary between Nubia and Somalia near 28° E		
Nubia–Antarctica	Spreading rates	43.8	50
Nubia–Antarctica	Transform fault azimuths	2.6	2
Nubia–Antarctica	Spreading rates and transform fault azimuths	55.8	54
Somalia–Antarctica	Spreading rates	52.0	47
Somalia–Antarctica	Transform fault azimuths	14.9	12
Somalia–Antarctica	Spreading rates and transform fault azimuths	82.5	61
	Narrow Boundary between Nubia and Somalia near 32.5° E		
Nubia–Antarctica	Spreading rates	41.1	50
Nubia–Antarctica	Transform fault azimuths	2.8	4
Nubia–Antarctica	Spreading rates and transform fault azimuths	61.3	56
Somalia–Antarctica	Spreading rates	52.0	47
Somalia–Antarctica	Transform fault azimuths	13.4	10
Somalia–Antarctica	Spreading rates and transform fault azimuths	82.4	59

A plate pair identifies two plates in relative motion across the SWIR. The African Plate is the entire region north of the SWIR from the Bouvet triple junction to the Rodrigues triple junction. The Nubian Plate lies west of 28°E and the Somalian Plate lies east of 28°E. Abbreviations: χ^2, sum-squared normalized misfit; ν, degrees of freedom.

The small values of chi-square indicate that the uncertainties for the transform fault azimuths determined using eq. (1) may be too conservative. There is less than a 2×10^{-4} chance of obtaining a value of chi-square this small or smaller if the uncertainties are estimated appropriately. We corrected for this possible overestimation of the uncertainties by multiplying the 1σ errors by 0.39, which is the square root of χ^2_ν (reduced chi-square, which is equal to chi-square divided by the number of degrees of freedom) for the best-fitting model. If we did not rescale the uncertainties, then transform fault azimuths would be weighted too lightly relative to spreading rates (which are already scaled to cause χ^2_ν to equal 1) in an analysis of the combined spreading rate and transform fault azimuth data. The rescaling has no effect on the best-fitting location or significance of the improvement in fit for our analysis of the transform fault azimuths alone.

Analysis of the dispersion of the fit to many transform faults on other plate boundaries suggests that our deliberately conservative method for estimating the uncertainties of transform fault azimuths tends to overestimate the uncertainties by approximately a factor of 2 (Argus & Gordon, unpublished analysis, 2003), similar to the factor we find herein.

4.1.3 Combined spreading rates and azimuths of transform faults

The spreading rates and transform fault azimuths were combined and the analysis was repeated. The smallest misfit ($\chi^2 = 138.3$,

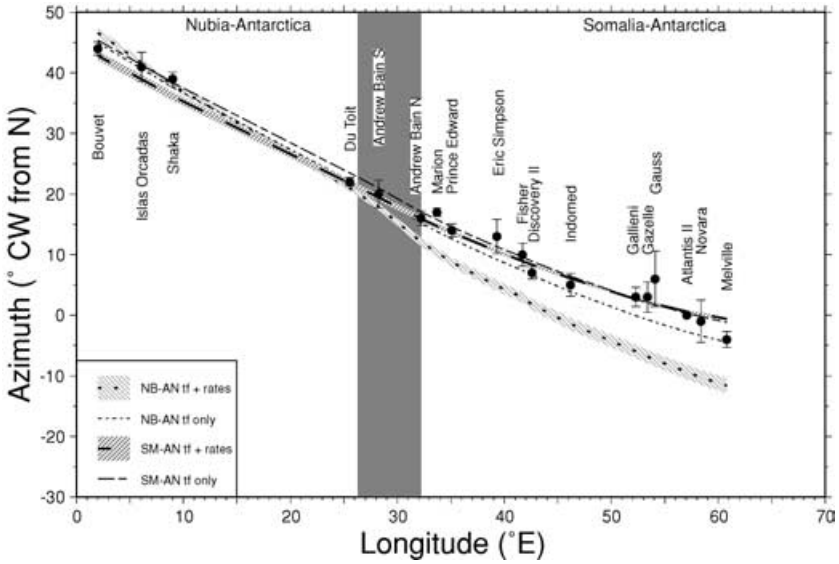

Figure 10. Comparison of observed transform fault azimuths with those calculated assuming a narrow Nubia–Somalia boundary intersecting the Southwest Indian ridge (SWIR) near 28°E. Dark grey shading shows the 95 per cent confidence limits of the best-fitting narrow Nubia–Somalia boundary. Dotted curve: azimuths calculated from the angular velocity (0.183° ± 0.012° Myr^{-1} about 13.0°S, 29.8°W) that best fits the spreading rates and transform fault azimuths west of 28°E, corresponding to Nubia–Antarctica motion; light grey diagonal stripes show 1σ uncertainty. Short dash-dot curve: azimuths calculated from the angular velocity that best fits the transform fault azimuths west of 28°E. Dashed curve: azimuths calculated from the angular velocity (0.131° ± 0.002° Myr^{-1} about 6.8°N, 42.5°W) that best fits the spreading rates and transform fault azimuths east of 28°E, corresponding to Somalia–Antarctica motion; dark grey diagonal stripes show 1σ uncertainty. Long dash-short dash curve: azimuths calculated from the angular velocity that best fits the transform fault azimuths east of 28° E.

$\nu = 114$) for the intersection of a hypothetical narrow Nubia–Somalia plate boundary with the SWIR is anywhere between the spreading rate located at 26.31°E and the azimuth of the southern portion of the ABTFC at 28.25°E (Figs 8, 9 and 10). At the best-fitting location, the data are fit significantly better ($F = 56.8$, with 4 versus 114 degrees of freedom, $p = 3 \times 10^{-26}$) by the three-plate model than by the Africa–Antarctica two-plate model ($\chi^2 = 413.7$, $\nu = 118$). The 95 per cent confidence limits for the best-fitting narrow boundary model (along the SWIR from 26.31°E to 32.24°E, excluding the endpoints) are slightly narrower than for the rates-only analysis (i.e. along the SWIR from 26.31°E to 32.89°E, excluding the endpoints).

If the Nubia–Somalia boundary is narrow and its location is not inferred from our plate motion data, but instead is specified by independent data, independent reasoning, or both, the fit to the data of the corresponding three-plate Nubia–Antarctica–Somalia model would be significantly better than the fit to a two-plate Africa–Antarctica model if chi-square for the three-plate model is below the thicker horizontal dashed line in Fig. 8. This criterion is satisfied by many hypothetical triple junction locations along nearly all of the SWIR (from 2.00°E to 66.00°E and 66.10°E to 66.15°E). In particular, if the Nubia–Somalia boundary is narrow and follows the inactive African continuation of the ABTFC, the data are fit significantly better ($F = 69.6$, with 3 versus 115 degrees of freedom, $p = 9.9 \times 10^{-26}$) by a three-plate model ($\chi^2 = 146.9$, $\nu = 115$) than by a two-plate model. If the Nubia–Somalia boundary is narrow and instead intersects the SWIR at the best-fitting Nubia–Somalia narrow boundary location of Chu & Gordon (1999; between 37.20°E and 38.50°E), the data are also fit significantly better ($F = 36.1$, with 3 versus 115 degrees of freedom, $p = 1.7 \times 10^{-16}$) by a three-plate model ($\chi^2 = 213.2$) than by a two-plate model (Table 3).

The values of chi-square are larger than expected and indicate that the spreading rates are inconsistent with the transform fault azimuths if we assume a narrow boundary between Nubia and Somalia ($p = 9.6 \times 10^{-6}$). This problem is less severe but still significant if we use the original (unrescaled) uncertainties for the transform fault azimuths ($p = 9.1 \times 10^{-3}$).

The inconsistency between spreading rates and transform fault azimuths in the combined data set occurs in both the Nubia–Antarctica and Somalia–Antarctica data subsets (Fig. 11). When the Nubia–Antarctica spreading rates ($\chi^2 = 43.8$, $\nu = 50$) and transform fault azimuths ($\chi^2 = 2.6$, $\nu = 2$) are analysed together ($\chi^2 = 55.8$), the misfit is significantly worse than when the two data types are analysed separately ($F = 5.2$, with 2 versus 52 degrees of freedom, $p = 8.6 \times 10^{-3}$). If we use the unrescaled uncertainties for the transform fault azimuths, the inconsistency is insignificant ($F = 1.4$, $p = 2.5 \times 10^{-1}$). Similarly, when the Somalia–Antarctica spreading rates ($\chi^2 = 52.0$, $\nu = 47$) and transform fault azimuths ($\chi^2 = 14.9$, $\nu = 12$) are analysed together ($\chi^2 = 82.5$), the misfit is significantly worse than when the two data types are analysed separately ($F = 6.9$, with 2 versus 59 degrees of freedom, $p = 2.0 \times 10^{-3}$). If we use the unrescaled uncertainties for the transform fault azimuths, the inconsistency is still significant ($F = 3.2$, $p = 4.8 \times 10^{-2}$).

Although the inconsistency between rates and transforms is statistically significant, the inconsistency is modest in size. If the standard deviation of both rates and transform fault azimuths were merely 10 per cent larger, the level of inconsistency would be exactly that expected statistically. We elected to make no correction for an inconsistency this small, while suspecting that it is caused by some correlation in the errors between spreading rates from closely spaced profiles.

4.2 Angular velocity of Nubia relative to Somalia; closure of the Arabia–Somalia–Antarctica–Nubia plate circuit

The best-fitting Nubia–Antarctica and Somalia–Antarctica angular velocities estimated from our best-fitting model respectively are 0.183° ± 0.012° Myr^{-1} about 13.0°S, 29.8°W and 0.131° ± 0.002° Myr^{-1} about 6.8°N, 42.5°W (Tables 4 and 5). They can be

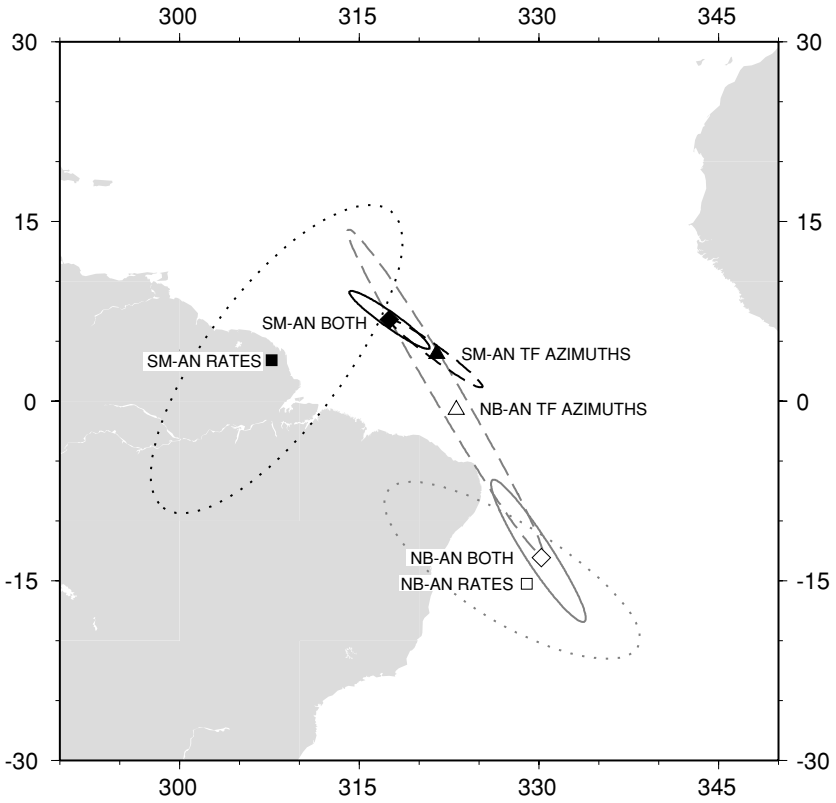

Figure 11. Nubia–Antarctica and Somalia–Antarctica poles of rotation for spreading rates only (squares), transform fault azimuths only (triangles), and combined spreading rates and transform fault azimuths (diamonds) assuming that a narrow Nubia–Somalia boundary intersects the Southwest Indian ridge (SWIR) near 28°E. Solid symbols indicate Somalia–Antarctica poles. Open symbols indicate Nubia–Antarctica poles. Ellipsoids show 95 per cent confidence regions.

Table 4. Best-fitting angular velocities.

Plate pair	Lat. (°N)	Lon. (°E)	ω (° Myr^{-1})	$\omega_{95\text{ per cent}}$	N	N_{rates}	N_{TF}	χ^2
Nubia–Antarctica	−13.0	−29.8	0.183	± 0.012	57	53	4	55.8
Somalia–Antarctica	6.8	−42.5	0.131	± 0.002	64	50	14	82.5
Arabia–Nubia	31.5	23.0	0.405	± 0.092	45	45	0	27.6
Arabia–Somalia	23.0	25.3	0.425	± 0.034	51	46	5	45.6

The angular velocities for each plate pair are the right-handed rotations of the first plate relative to the second plate. The Nubia–Antarctica and Somalia–Antarctica angular velocities are estimated from spreading rates and transform fault azimuths along the SWIR, assuming the best-fitting Nubia–Somalia boundary near ≈28°E along the SWIR. The Arabia–Nubia angular velocity is estimated from spreading rates in the Red sea, and the Arabia–Somalia angular velocity is estimated from spreading rates and transform fault azimuths in the Gulf of Aden (Chu & Gordon 1998, 1999). Abbreviations: lat., latitude; lon., longitude; ω, angular speed; $\omega_{95\text{ per cent}}$, 95 per cent confidence limits on the angular speed; N, number of data used to estimate the angular velocity; N_{rates}, number of spreading rates used to estimate the angular velocity; N_{TF}, number of transform fault azimuths used to estimate the angular velocity; χ^2, sum-squared normalized misfit.

Table 5. Covariance matrices for best-fitting and closure enforced angular velocities.

Plate pair	Type	xx	xy	xz	yy	yz	zz
Nubia–Antarctica	Best fit	101.8	29.3	−135.2	10.8	−38.0	190.4
Somalia–Antarctica	Best fit	8.4	9.8	−9.0	16.6	−13.7	12.8
Arabia–Nubia	Best fit	3373.4	3004.2	1796.3	2914.5	1810.9	1149.9
Arabia–Somalia	Best fit	478.4	529.7	102.7	597.5	120.5	52.9
Nubia–Antarctica	Closure	44.8	12.9	−55.8	6.0	−15.2	79.9
Somalia–Antarctica	Closure	7.9	8.8	−8.2	14.9	−12.2	11.5
Arabia–Nubia	Closure	171.1	193.2	120.5	266.8	180.9	132.6
Arabia–Somalia	Closure	274.8	298.9	70.7	335.5	84.0	47.1

Plate pairs as in Tables 4 and 8. Type is the type of angular velocity: best fit is the best-fitting two-plate angular velocity, closure is the angular velocity when closure is enforced in a closed four-plate circuit such as Nubia–Arabia–Somalia–Antarctica. Abbreviations: xx, xy, xz, yy, yz and zz are components of a symmetric 3 × 3 covariance matrix. Units of the elements of the matrix are 10^{-10} sr Myr^{-2}. x parallels 0°N, 0°E; y parallels 0°N, 90°E; and z parallels 90°N.

Table 6. Nubia–Somalia angular velocities.

Boundary location	Number of plates	Lat. (°N)	Lon. (°E)	ω (° Myr^{-1})	N	N_{rates}	N_{TF}	χ^2
28°E	3	−44.0	−0.7	0.082	121	103	18	138.3
28°E	4	−44.7	2.8	0.084	217	194	23	246.3
ABTFC	3	−41.6	−1.7	0.071	121	103	18	146.9
ABTFC	4	−43.4	4.0	0.080	217	194	23	255.1

Models labelled 28°E and ABTFC assume a hypothetical narrow boundary between Nubia and Somalia that intersects the Southwest Indian ridge (SWIR), respectively near 28°E and along the inactive African continuation of the Andrew Bain transform fault complex (ABTFC; near 32.2°E). If the number of plates is three, which corresponds to the Nubia, Antarctica and Somalia plates, then only data along the SWIR were used to estimate the angular velocities. If the number of plates is four, which corresponds to the same three plates plus the Arabian Plate, the data from the Red sea and Gulf of Aden (Chu & Gordon 1998, 1999) were used, along with data along the SWIR, to estimate angular velocities. Abbreviations: lat., latitude; lon., longitude; ω, angular speed; N, number of data used to estimate the angular velocity; N_{rates}, number of spreading rates used to estimate the angular velocity; N_{TF}, number of transform fault azimuths used to estimate the angular velocity; χ^2, sum-squared normalized misfit.

Table 7. Covariance matrices for Nubia–Somalia angular velocities.

Boundary location	Number of plates	xx	xy	xz	yy	yz	zz
28°E	3	110.3	39.1	−144.2	27.4	−51.7	203.2
28°E	4	42.9	12.6	−50.1	16.2	−14.4	71.9
ABTFC	3	100.1	38.8	−125.9	29.7	−50.0	171.0
ABTFC	4	42.0	13.4	−47.9	17.6	−15.4	66.1

Models are as in Table 6. Abbreviations: xx, xy, xz, yy, yz and zz are components of a symmetric 3 × 3 covariance matrix. Units of the elements of the matrix are 10^{-10} sr Myr^{-2}. x parallels 0°N, 0°E; y parallels 0°N, 90°E; and z parallels 90°N.

Table 8. Closure enforced angular velocities.

Plate pair	Lat. (°N)	Lon. (°E)	ω (° Myr^{-1})
Nubia–Antarctica	−12.8	−29.9	0.182 ± 0.012
Somalia–Antarctica	7.9	−44.1	0.133 ± 0.002
Arabia–Nubia	36.7	25.9	0.366 ± 0.024
Arabia–Somalia	24.6	22.1	0.384 ± 0.025
Nubia–Somalia	−44.7	2.8	0.084 ± 0.012

The angular velocities for each plate pair are the right-handed rotations of the first plate relative to the second plate. Abbreviations: lat., latitude; lon., longitude; ω, angular speed and its 95 per cent confidence limits.

differenced to estimate the angular velocity of Nubia relative to Somalia of 0.082° ± 0.020° Myr^{-1} about 44.0°S, 0.7°W (Tables 6 and 7). When the plate motion data along the SWIR are combined with Nubia–Arabia data from the Red sea (45 spreading rates) and with Somalia–Arabia data from the Sheba ridge in the Gulf of Aden (46 spreading rates and five transform fault azimuths), the Nubia–Somalia angular velocity is estimated to be 0.084° ± 0.012° Myr^{-1} about 44.7°S, 2.8°E (from the four-plate Arabia–Nubia–Antarctica–Somalia circuit; Fig. 1; Tables 5, 6, 7 and 8).

Chi-square for the combined four-plate Arabia–Somalia–Antarctica–Nubia plate motion circuit ($\chi^2 = 246.3$ with 208 degrees of freedom) is significantly greater than the sum of chi-square for the four best-fitting angular velocities (Somalia–Arabia, Nubia–Arabia, Somalia–Antarctica and Nubia–Antarctica; combined $\chi^2 = 211.3$ with 208 degrees of freedom; $F = 11.7$ with 3 versus 205 degrees of freedom, $p = 4.3 \times 10^{-7}$). Thus, the four best-fitting angular velocities are not mutually consistent. This inconsistency is illustrated in Fig. 12, which shows that our Nubia–Somalia angular velocity estimated from data only along the SWIR differs significantly from the Nubia–Somalia angular velocity estimated from Red sea and Gulf of Aden data.

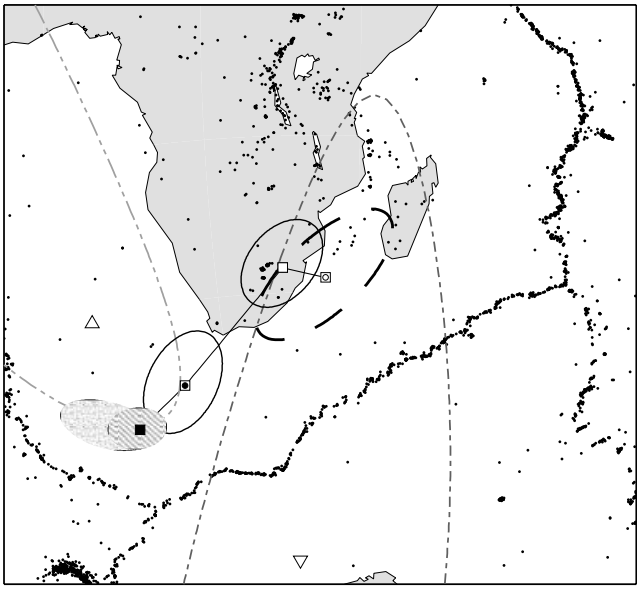

Figure 12. Various estimated Nubia–Somalia angular velocities. The two black-filled symbols show results using our new data. Triangle: our new Nubia–Somalia pole of rotation using data only along the Southwest Indian ridge (SWIR). Square: our new Nubia–Somalia pole of rotation using data along the SWIR, from the Gulf of Aden and from the Red sea. The other symbols show results using the data set of Chu & Gordon (1999). Open inverted triangle: Nubia–Somalia pole of rotation from data in the Red sea and Gulf of Aden. Open triangle: Nubia–Somalia pole of rotation using data only along the SWIR assuming the same location of the Nubia–Somalia–Antarctica triple junction found herein. Squares: Nubia–Somalia poles of rotation from data along the SWIR, from the Gulf of Aden and from the Red sea (open square with open circle, diffuse Nubia–Somalia boundary between 32.99°E and 52.32°E; open square, narrow Nubia–Somalia boundary intersecting the SWIR near 38°E; open square with solid circle, narrow Nubia–Somalia boundary intersecting the SWIR along the inactive African continuation of the Andrew Bain transform fault complex, ABTFC). Small black-filled circles: earthquake epicentres (1964–1998; Engdahl *et al.* 1998).

In the four-plate inversion, the Nubia–Antarctica, Somalia–Antarctica and Somalia–Arabia angular velocities change little from their best-fitting values, but the Nubia–Arabia angular velocity from the four-plate circuit differs significantly from the corresponding best-fitting angular velocity (Fig. 13). The Red sea has no useful transform fault azimuths. The sum of the best-fitting Nubia–Antarctica, Antarctica-Somalia and Somalia–Arabia angular velocities predicts a Nubia–Arabia pole of rotation east-northeast of

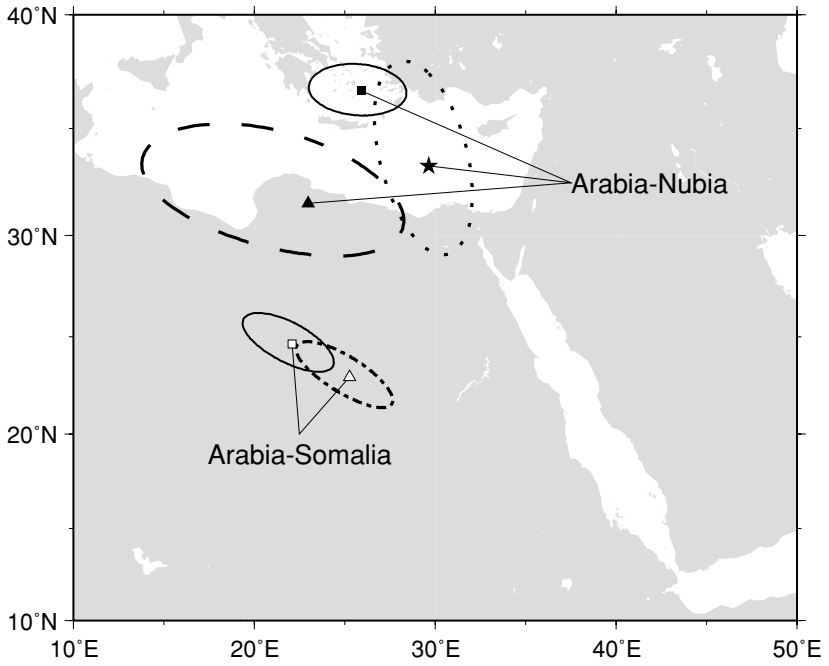

Figure 13. Location of Arabia–Nubia and Arabia–Somalia poles of rotation and 95 per cent confidence regions. Open triangle: Arabia–Somalia pole of rotation estimated from only data in the Gulf of Aden. Solid triangle: Arabia–Nubia pole of rotation estimated from only data in the Red sea. Squares: Arabia–Nubia (solid) and Arabia–Somalia (open) poles of rotation estimated from data from the Red sea, Gulf of Aden and Southwest Indian ridge (SWIR), assuming the best-fitting narrow Nubia–Somalia boundary intersects the SWIR near 28°E. Star: Arabia–Nubia pole of rotation predicted by summing the Arabia–Somalia, Somalia–Antarctica and Antarctica–Nubia best-fitting angular velocities.

the best-fitting pole of rotation, predicting a direction of motion clockwise of that indicated by the best-fitting pole (Fig. 13). The closure-enforced pole also indicates a more clockwise direction of motion (Fig. 13).

4.3 Linear velocities of Somalia relative to Nubia

We determine Nubia–Somalia linear velocities from two different estimates of the angular velocity of Somalia relative to Nubia: (i) the angular velocity determined only from data along the SWIR, and (ii) the angular velocity that also incorporates data from the Red sea and Gulf of Aden. Below the latter is given parenthetically. Near the Afar triple junction (i.e. at 10.0°N, 40.0°E), the displacement rate of Somalia relative to Nubia is 8.3 ± 1.9 mm yr^{-1} towards $121° \pm 5°$ (8.4 ± 1.2 mm yr^{-1} towards $119° \pm 3°$). The total displacement since 3.2 Ma is 27 ± 6 km (27 ± 4 km).

Lemaux *et al.* (2002) reported a displacement rate of 2.1 ± 0.5 mm yr^{-1} towards 188° relative to Nubia for a Somalian Plate location at 46.5°S, 33.3°E, just east of the African continuation of the ABTFC. Our estimate of the displacement rate is 3.6 ± 0.5 mm yr^{-1} towards $176° \pm 6°$ (3.3 ± 0.5 mm yr^{-1} towards $176° \pm 6°$). The estimate of the total displacement since 11 Ma of Lemaux *et al.* (2002) is 23 ± 6 km. Our estimate of the total displacement over 3.2 Ma for the same location is 11.5 ± 1.6 km, approximately half of, and significantly less than, the motion since 11 Ma, indicating that motion before 3.2 Ma is required.

5 DISCUSSION

5.1 Sensitivity of pole of rotation to assumed triple junction location

The pole of rotation obtained herein lies far outside the confidence region of the pole of rotation of Chu & Gordon (1999). Such a result would be unlikely if the confidence region of Chu & Gordon (1999) fully incorporated all sources of uncertainty. Here, we investigate the effect on the pole location of the difference in the data set and the assumed difference in triple junction location along the SWIR between Chu & Gordon's (1999) results and ours.

We first constructed three estimates of the Nubia–Somalia angular velocities determined from Chu & Gordon's (1999) data along the SWIR, the Sheba ridge (Gulf of Aden) and the Red sea spreading centre, as follows:

(i) assuming a diffuse boundary between 32.99°E and 52.32°E, as assumed by Chu & Gordon (1999);

(ii) assuming a narrow boundary at ≈38°E, as alternatively assumed by Chu & Gordon (1999); and

(iii) assuming a narrow boundary along the inactive African continuation of the ABTFC, as proposed by Lemaux *et al.* (2002).

Model (iii) is equivalent to our best-fitting model, as Chu & Gordon (1999) had no plate motion data between our best-fitting location and the inactive African continuation of the ABTFC. Moreover, models (ii) and (iii) differ only in shifting merely three of Chu & Gordon's (1999) data from the Nubia–Antarctica to the Somalia–Antarctica plate boundary.

The resulting poles of rotation differ considerably (Fig. 12). The two narrow boundary models, (ii) and (iii), differ significantly from one another, despite differing only in the plate boundary assignments of three data. The angular velocity estimated assuming a narrow boundary along the inactive African continuation of the ABTFC is similar to our new angular velocity. Thus, a large part of the difference between Chu & Gordon's (1999) pole of rotation and ours may be caused by assuming a different location for the triple junction. If Chu & Gordon's (1999) confidence region had incorporated this

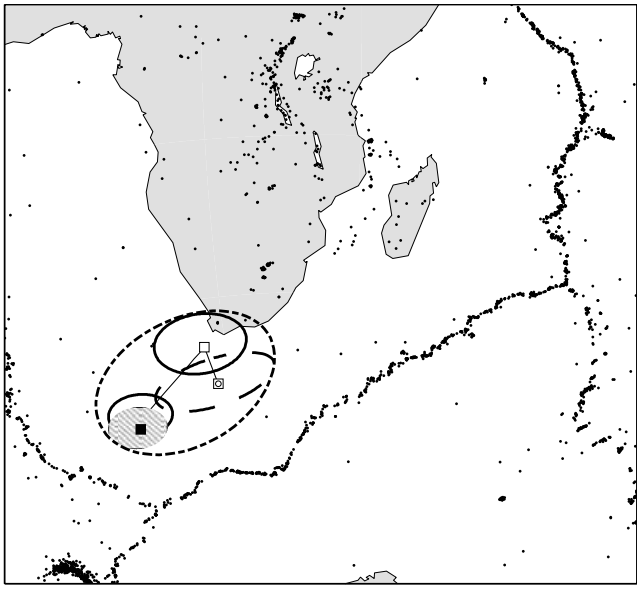

Figure 14. Illustration of the insensitivity of our new estimated Nubia–Somalia angular velocity to the assumed location of the Nubia–Antarctica–Somalia triple junction along the Southwest Indian ridge (SWIR), using our data along the SWIR and the same assumed boundary locations as in Fig. 12. Squares: Nubia–Somalia poles of rotation and surrounding 95 per cent confidence limits (open square with open circle, diffuse Nubia–Somalia boundary between 32.99°E and 52.32°E; open square, narrow Nubia–Somalia boundary intersecting the SWIR near 38°E; open square with solid circle, narrow Nubia–Somalia boundary intersecting the SWIR along the inactive African continuation of the Andrew Bain transform fault complex, ABTFC; black square, boundary intersecting ABTFC between the locations of the two observed azimuths). Black dash-dot curve: ellipse that includes the 95 per cent confidence limits of the four models shown here. Small black-filled circles: earthquake epicentres (1964–1998; Engdahl *et al.* 1998).

further uncertainty, then our new result would be consistent with theirs.

How sensitive is our new angular velocity to changes in the assumed location of the Nubia–Somalia boundary near the SWIR? Fig. 14 shows results analogous to those of Fig. 12 except that our new data are used instead of those of Chu & Gordon (1999). The results show that the location of the pole of rotation depends on the assumed plate boundary location, but much less so than for Chu & Gordon's (1999) data. Thus, our new estimated angular velocity seems reasonably robust with respect to the assumed location of the plate boundary. An ellipsoidal envelope enclosing the four ellipsoids shown in Fig. 14 gives a more conservative 95 per cent confidence region for the Nubia–Somalia pole of rotation than does the ellipsoid for the model for the best-fitting boundary.

5.2 Comparison with results for magnetic anomaly 5 (11 Ma)

Unlike the results of Chu & Gordon (1999), the results we obtain here are consistent or nearly consistent with those of Lemaux *et al.* (2002). Our inferred limits on the location of the intersection of the Nubia–Somalia boundary with the SWIR are similar to and slightly narrower than those of Lemaux *et al.* (2002). Moreover, our inferred pole of rotation, which has much more compact limits than those of Lemaux *et al.* (2002), slightly overlaps that of Lemaux *et al.* (2002; Fig. 15). We find this improved consistency encouraging.

5.3 Oceanic Nubia–Somalia boundary: narrow or diffuse?

Although our results are consistent with the Nubia–Somalia boundary being narrow between the East African rift and the SWIR, there is no strong evidence that this is so. In particular, there is no narrow topographic feature or line of earthquakes, as observed for example along the slow slipping Owen fracture zone (Gordon & DeMets 1989). Moreover, as its azimuth shows that the Nubia–Somalia boundary must intersect the SWIR southwest of the northern part of the ABTFC, it follows that the Nubia–Somalia boundary cannot precisely follow the inactive African continuation of the ABTFC near the SWIR, as proposed by Lemaux *et al.* (2002). The data also limit the intersection of the Nubia–Somalia boundary with the SWIR to east of ≈26°E, which permits a diffuse boundary as wide as 700 km near the SWIR.

Because of the absence of seismicity and topographic features, it is unclear how the East African rift connects to the triple junction along the SWIR. Fig. 15 shows one possibility inspired by the diffuse oceanic plate boundaries in the Indo-Australian composite plate (Royer & Gordon 1997; Gordon 1998). The East African rift is shown as being transformed into a diffuse contractional oceanic plate boundary near the pole of rotation, instead of following the shortest distance between the rift and triple junction along the SWIR. Fig. 16 shows another possibility, the shortest distance solution, for a boundary that is ≈700 km wide near the SWIR and broadens to ≈1000 km wide near the east coast of southern Africa.

Earthquakes off the ridge axis occur between the SWIR and Africa (Fig. 16; Table 9), but none with a published focal mechanism occurs between Africa and the Nubia–Antarctica part of the SWIR. The largest earthquakes off the ridge axis occur between 41°E and 49°E with a cluster near 37°S, 48°E, suggesting that some Nubia–Somalia motion may be accommodated over a much wider zone than indicated by our analysis of the plate motion data or also in a second locus of deformation. This is also suggested by the distribution of earthquakes, which continues as far eastwards as Madagascar (see, e.g. Fig. 15). The earthquakes, combined with the significant non-closure of the Arabia–Somalia–Antarctica–Nubia plate motion circuit, strongly suggest that what we herein treat as a single rigid Somalian Plate is not rigid. Perhaps the Somalian component plate actually consists of multiple plates as suggested by Hartnady (2002), or perhaps it contains a large diffuse plate boundary with a slow rate of deformation.

It is of interest that the focal mechanisms of the earthquakes near the ridge axis all have similar *P* axes indicating approximately NE–SW contraction (Fig. 16). The largest magnitude earthquake off the ridge axis is the $M_w = 6.8$ thrust-faulting event of 1988 February 26. Thus the seismicity provides no support for the proposed location of our narrow plate boundary, but by themselves the earthquakes are too sparse to convincingly deny the hypothesis.

6 CONCLUSIONS

A boundary between Nubia and Somalia intersects the SWIR. Our results, taken together with those of Lemaux *et al.* (2002), indicate that the boundary may be narrow (i.e. no more than a few tens of kilometres wide) or up to ≈700 km wide. The boundary intersects the SWIR between 26.3°E and 32.2°E, east of a spreading rate observed east of the Du Toit transform fault but southwest of the northernmost part of the ABTFC. The boundary cannot precisely follow the inactive African continuation of the Andrew Bain transform fault near the SWIR and must lie west of it. Because of the lack of expression in topography and seismicity, it is unclear where

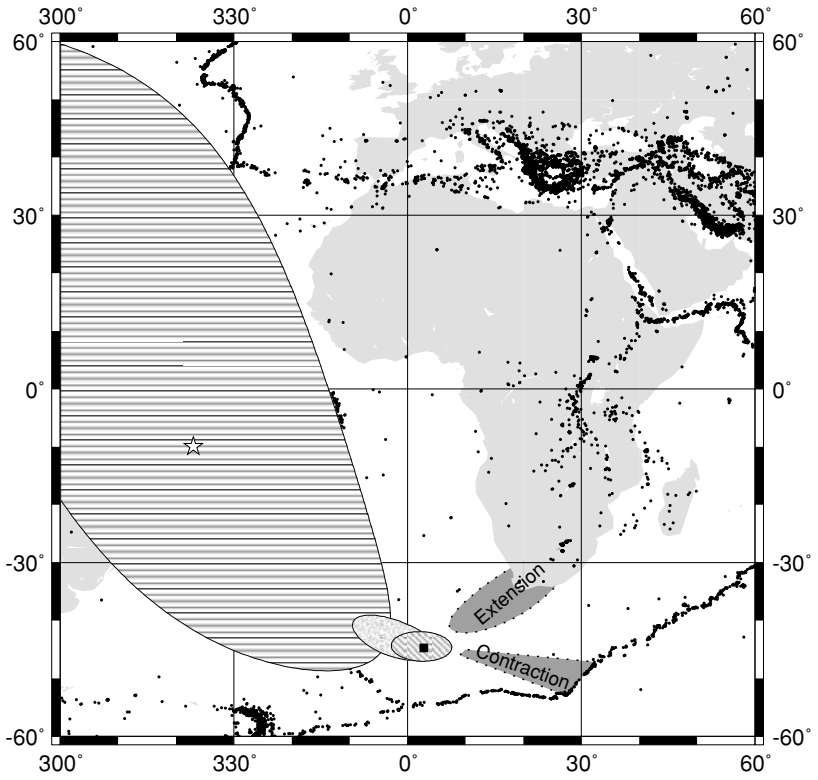

Figure 15. Comparison of Nubia–Somalia (NB–SM) motion since 3.2 Ma (anomaly 2A) with that since 11 Ma (anomaly 5). Both estimates assume a narrow NB–SM boundary intersecting the Southwest Indian ridge (SWIR) near 28°E. Triangle and stippled ellipsoid: NB–SM pole and 95 per cent confidence region estimated from spreading rates and transform fault azimuths along the SWIR. Square and diagonally striped ellipsoid: NB–SM pole and 95 per cent confidence region estimated from data along the SWIR, the Red sea and Gulf of Aden. Star and horizontally striped ellipsoid: NB–SM pole and 95 per cent confidence region estimated from finite rotations of magnetic anomaly 5 across the SWIR (Lemaux *et al.* 2002). Dark grey shaded regions: possible locations for extensional and contractional diffuse oceanic plate boundaries near the poles of rotation. Small black-filled circles: earthquake epicentres (1964–1998; Engdahl *et al.* 1998).

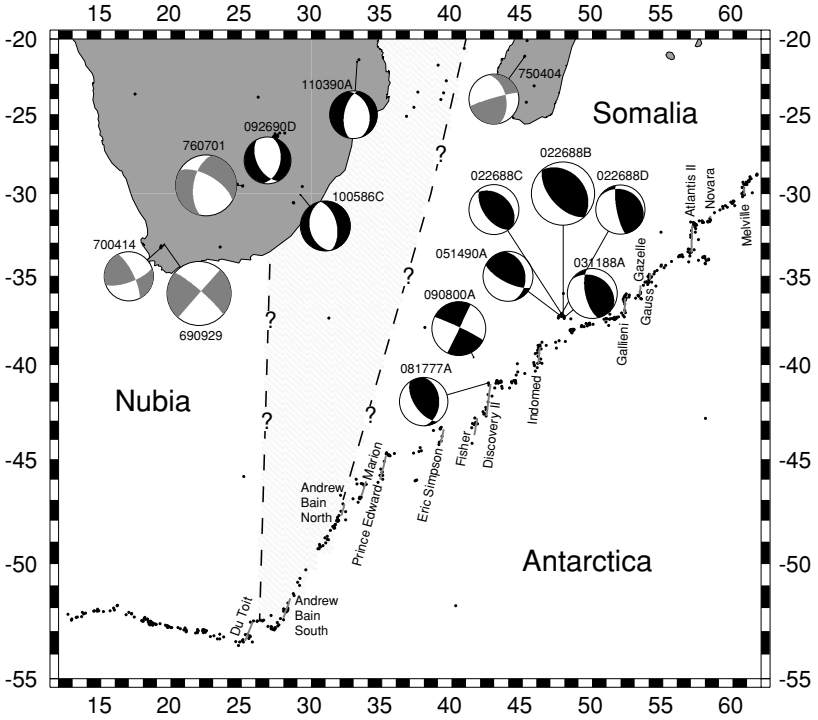

Figure 16. Off-ridge-axis focal mechanisms and possible Nubia–Somalia plate boundary. The region shaded light grey shows a possible location of a boundary that is ≈700 km wide near the Southwest Indian ridge (SWIR) and ≈1000 km wide near the east coast of southern Africa. Focal mechanisms are shaded black and white if from the Harvard centroid-moment-tensor catalogue and grey and white if from Shudofsky (1985). Grey lines: observed transform faults. Black dots: earthquake epicentres (1964–1998; Engdahl *et al.* 1998).

Table 9. Focal mechanisms for intraplate seismicity between Africa and the Southwest Indian ridge (SWIR).

Date	Time (UTC)	Lat. (° N)	Lon. (° E)	m_b	M_w	Strike (°)	Dip (°)	Slip (°)	Type
1969.09.29	20:03:32.1	−33.09	19.52	5.6	—	311	82	180	Strike-slip
1970.04.14	19:08:21.8	−33.17	19.47	5.4	—	334	74	160	Strike-slip
1975.04.04	17.31.16.1	−21.24	45.13	5.3	—	254	85	140	Strike-slip
1976.07.01	11:24:04.7	−29.51	25.17	5.9	—	300	63	219	Normal
1977.08.17	10:41:44.7	−40.81	43.35	5.1	5.2	145	58	70	Thrust
1986.10.05	18:53:20.9	−30.55	28.87	4.9	4.8	168	37	270	Normal
1988.02.26	06:17:41.2	−36.88	48.03	6.1	6.8	318	33	89	Thrust
1988.02.26	13:42:33.9	−36.45	47.93	5.4	5.3	310	35	79	Thrust
1988.02.26	17:52:39.8	−36.87	48.21	5.4	5.3	298	20	41	Thrust
1988.11.03	02:37:03.8	−36.90	48.17	5.4	5.3	303	31	51	Thrust
1990.05.14	06:52:15.6	−37.13	48.11	5.3	5.4	117	70	64	Thrust
1990.09.26	23:08:24.1	−28.05	26.69	5.6	4.7	11	45	299	Normal
1990.11.03	00:31:29.3	−21.37	33.15	5.0	5.1	345	35	249	Normal
2000.09.08	01:34:45.4	−39.60	41.55	5.6	5.8	295	86	359	Strike-slip

The first four focal mechanisms are from Shudofsky (1985) and the rest are from the Harvard CMT catalogue. Abbreviations: UTC, Coordinated Universal Time; lat., latitude; lon., longitude; m_b, body wave magnitude; M_w, moment magnitude.

the boundary lies between the East African rift and its intersection with the SWIR.

The pole of rotation of Nubia relative to Somalia lies southwest of southern Africa and has usefully compact confidence limits. The new angular velocity is much less sensitive to the assumed location and width of the Nubia–Somalia boundary where it intersects the SWIR than was the angular velocity estimated by Chu & Gordon (1999). The new Nubia–Somalia pole of rotation is in better agreement with the anomaly 5 pole of rotation (Lemaux *et al.* 2002) than is the pole of rotation of Chu & Gordon (1999).

On the other hand, the Nubia–Somalia angular velocity estimated from data along the SWIR is inconsistent with the angular velocity estimated from data in the Red sea and Gulf of Aden. Moreover, the boundary that we find here lies far west (i.e. near 30°E) of the sparse off-ridge earthquakes that may record deformation as a result of motion between Nubia and Somalia, in particular the $M_w = 6.8$ event near 48°E (Fig. 16). The boundary we find here also lies near the western edge of seismicity indicating east–west extension across southern Africa, the Mozambique channel and Madagascar (Figs 14 and 16). Thus, it seems likely that the Somalian component plate is non-rigid and may include one or more broad zones of deformation, one or more smaller component plates, or both. We are currently investigating these hypotheses.

ACKNOWLEDGMENTS

All figures were prepared using GMT (Wessel & Smith 1998). We thank John Sclater and Bob Fisher for making unpublished bathymetric data available to us. This work was supported by National Science Foundation grants OCE9819365, EAR9903763 and OCE0242905. Donald Argus's part of this research was performed at the Jet Propulsion Laboratory, California Institute of Technology, under contract with the National Aeronautics and Space Administration.

REFERENCES

Baker, B.H., 1972. Geology of the Eastern Rift system of Africa, *Geol. Soc. Am. Bull.,* **186,** 1–67.

Cande, S.C. & Kent, D.V., 1995. Revised calibration of the geomagnetic polarity timescale for the Late Cretaceous and Cenozoic, *J. geophys. Res.,* **100,** 6093–6095.

Chang, T., 1988. Estimating the relative rotation of two tectonic plates from boundary crossings, *J. Am. Stat. Assoc.,* **83,** 1178–1183.

Chase, C.G., 1978. Plate kinematics: The Americas, East Africa, and the rest of the world, *Earth planet. Sci. Lett.,* **37,** 355–368.

Chu, D. & Gordon, R.G., 1998. Current plate motions across the Red Sea, *Geophys. J. Int.,* **135,** 313–328.

Chu, D. & Gordon, R.G., 1999. Evidence for motion between Nubia and Somalia along the Southwest Indian Ridge, *Nature,* **398,** 64–67.

DeMets, C., Gordon, R.G., & Argus, D.F., 1988. Intraplate deformation and closure of the Australia-Antarctica-Africa plate circuit, *J. geophys. Res.,* **93,** 11 877–11 897.

DeMets, C., Gordon, R.G., Argus, D.F. & Stein, S., 1990. Current plate motions, *Geophys. J. Int.,* **101,** 425–478.

DeMets, C., Gordon, R.G. & Vogt, P., 1994. Location of the Africa-Australia-India triple junction and motion between the Australian and Indian plates: results from an aeromagnetic investigation of the Central Indian and Carlsberg ridges, *Geophys. J. Int.,* **119,** 893–930.

Dick, H.J.B. *et al.*, 1991. Tectonic evolution of the Atlantis II Fracture Zone, *Proc. ODP, Sci. Res.,* **118,** 359–398.

Engdahl, E.R., van der Hilst, R. & Buland, R., 1998. Global teleseismic earthquake relocation with improved travel times and procedures for depth determination, *Bull. seism. Soc. Am.,* **88,** 722–743.

Fairhead, J.D. & Stuart, G.W., 1982. The seismicity of the East African Rift system and comparison with other continental rifts, in, *Continental and Oceanic Rifts,* Geodynamics Series Vol. 8, pp. 41–61, ed. Palmason, G., AGU/GSA, Washington DC, USA.

Fisher, R. L. & Goodwillie, A. M., 1997. The Physiography of the Southwest Indian Ridge, *Mar. Geophys. Res.,* **19,** 451–455.

Gordon, R.G., 1998. The plate tectonic approximation: Plate nonrigidity, diffuse plate boundaries, and global plate reconstructions, *Annu. Rev. Earth Pl. Sc.,* **26,** 615–642.

Gordon, R.G. & DeMets, C., 1989. Present-day motion along the Owen fracture zone and Dalrymple Trough in the Arabian Sea, *J. geophys. Res.,* **94,** 5560–5570.

Hartnady, C.J.H., 2002. Earthquake hazard in Africa: perspectives on the Nubia–Somalia boundary, *S. Afr. J. Sci.* **98,** 425–428.

Jestin, F., Huchon, P. & Gaulier, J.M., 1994. The Somalia plate and the East African Rift System: present-day kinematics, *Geophys. J. Int.,* **116,** 637–654.

Lemaux, J., Gordon, R.G. & Royer, J.-Y., 2002. The location of the Nubia–Somalia boundary along the Southwest Indian Ridge, *Geology,* **30,** 339–342.

Ligi, M. *et al.*, 1999. Bouvet Triple Junction in the South Atlantic: Geology and evolution, *J. geophys. Res.,* **104,** 29 365–29 385.

Mendel, V., Sauter, D., Parson, L. & Vanney, J.-R., 1997. Segmentation and morphotectonic variations along a super slow-spreading center; the Southwest Indian Ridge (57 degrees E—70 degrees E), *Mar. Geophys. Res.,* **19,** 505–533.

Mohr, P. A., 1987. Structural style of continental rifting in Ethiopia: reverse decollements, *EOS, Trans. Am. geophys. Un.,* **68,** 721.

Morley, C.K., Wescott, W.A., Stone, D.M., Harper, R.M., Wigger, S.T. & Karanja, F.M., 1992. Tectonic evolution of the Northern Kenyan Rift, *J. geol. Soc. Lond.,* **149,** 333–348.

Royer, J.-Y. & Gordon, R.G., 1997. The motion and boundary between the Capricorn and Australian plates, *Science,* **277,** 1268–1274.

Sclater, J.G., Munschy, M., Fisher, R.L., Weatherall, P., Cande, S.C., Patriat, P., Bergh, H. & Schlich, R., 1997. *Geophysical Synthesis of the Indian/Southern Oceans: Part 1, The Southwest Indian Ocean,* Vol. 97-6, Scripps Institution of Oceanography, La Jolla, California, USA.

Shudofsky, G.N., 1985. Source mechanisms and focal depths of east African earthquakes using Rayleigh-wave inversion and bodywave modelling, *Geophys. J. R. astr. Soc.,* **83,** 563–614.

Smith, W.H.F. & Sandwell, D., 1997. Global seafloor topography from satellite altimetry and ship depth soundings, *Science,* **277,** 1955–1962.

Stein, S. & Gordon, R.G., 1984. Statistical tests of additional plate boundaries from plate motion inversions, *Earth planet. Sci. Lett.,* **69,** 401–412.

Wessel, P. & Smith, W., 1998. New, improved version of the Generic Mapping Tools released, *EOS, Trans. Am. geophys. Un.,* **79,** 579.